Ab initio ground potential energy surface, VTST and QCT study of the $O(^3P)+CH_4(X\,^1A_1)\rightarrow OH(X\,^2\Pi)+CH_3(X\,^2A_2'')$ reaction

Miguel González[a] and Jordi Hernando
Departament de Química Física, Universitat de Barcelona, Martí i Franquès, 1. 08028 Barcelona, Spain

Judith Millán
Departamento de Química, Universidad de La Rioja, Obispo Bustamante, 3. 26004 Logroño, Spain

R. Sayós[a]
Departament de Química Física, Universitat de Barcelona, Martí i Franquès, 1. 08028 Barcelona, Spain

(Received 13 July 1998; accepted 15 January 1999)

An *ab initio* study of the ground potential energy surface (PES) of the $O(^3P)+CH_4\rightarrow OH+CH_3$ reaction has been performed using the second- and fourth-order Møller–Plesset methods with a large basis set. A triatomic analytical ground PES with the methyl group treated as an atom of 15.0 a.m.u. has been derived. This PES has been employed to study the kinetics [variational transition state theory (VTST) and quasiclassical trajectory (QCT) rate constants] and dynamics (QCT method) of the reaction. The *ab initio* points have also been used directly to calculate the VTST rate constant considering all atoms of the system. The best VTST methods used lead to a good agreement with the experimental rate constant for 1000–2500 K, but QCT rate constant values are about one-third the experimental ones for 1500–2500 K. The cold QCT $OH(v=0)$ rotational distribution arising from the simulation of the reaction with $O(^3P)$ atoms produced in the photodissociation of NO_2 at 248 nm is in good agreement with experiment, while the very small QCT $OH(v=1)$ population obtained is consistent with measurements. The triatomic PES model derived in this work may be used in studies of the kinetics and dynamics under conditions where the methyl group motions are not strongly coupled to the motions leading to reaction. © *1999 American Institute of Physics.* [S0021-9606(99)00215-9]

I. INTRODUCTION

The reaction with ground-state atomic oxygen, $O(^3P)$, is an important initial step of hydrocarbon oxidation in combustion processes.[1] Among these reactions, the gas-phase bimolecular reaction

$$O(^3P)+CH_4(X\,^1A_1)\rightarrow OH(X\,^2\Pi)+CH_3(X\,^2A_2'')$$

$$\Delta H^0_{298\ K}=2.480\ \ \text{kcal mol}^{-1}\ ^2 \qquad (1)$$

may play an important role in obtaining a deep insight into the dynamics of this type of process. Because of its relative simplicity, as compared to other reactions with larger hydrocarbon molecules, it allows for a strong interaction between theory and experiment. In spite of its interest, however, to the best of our knowledge, only two experimental investigations have been devoted to the study of the dynamics of reaction (1). This has probably been caused by the fact that, among the different hydrocarbon reactions, the reaction with methane presents the highest barrier height between reactants and products, and it is difficult to generate $O(^3P)$ atoms with high enough translational energy to overcome this energy requirement.

Regarding the experimental studies, the ν_2 out-of-plane bending (''umbrella'' mode) vibrational distribution of CH_3 from reaction (1) was determined[3] in an infrared diode laser absorption kinetic spectroscopy experiment, with translationally hot $O(^3P)$ atoms generated by laser photolysis of SO_2 at 193 nm [average relative translational energy (E_T) of 0.330 eV]. More recently, several properties of the title reaction were characterized in an experiment,[4] combining laser photolysis of NO_2 at 248 nm to produce translationally hot $O(^3P)$ atoms (average E_T of 0.348 eV) with laser-induced fluorescence (LIF) detection of the nascent $OH(X\,^2\Pi)$ product: rotational distribution of $OH(X\,^2\Pi_{3/2},v'=0)$, and $OH(v'=0)$ Λ-doublet components and spin-orbit population ratios ($^2\Pi_{3/2}/^2\Pi_{1/2}$). With respect to the kinetics, the thermal rate constant (k) of reaction (1) has been measured[5–10] at different temperatures.

Reaction (1) has also been studied theoretically. Nonadiabatic coupling models for OH spin-orbit ($^2\Pi_{3/2}$,$^2\Pi_{1/2}$) propensities have been proposed[11] and *ab initio* calculations at different levels[12–15] have been reported. These calculations were mainly centered on the determination of the saddle point geometry and energy, and conventional transition state theory (TST) rate constants were also calculated in some cases.[12,13] A dual-level direct dynamics calculation of the rate constant of reaction (1) and of the analogous reaction with CD_4 has also been reported very recently.[15]

There is also a considerable body of work devoted to the experimental characterization (via molecular beams with LIF detection of products) of the $OH(X\,^2\Pi)$ molecules produced in related processes, like the reactions of $O(^3P)$ with

[a]Authors to whom correspondence should be addressed; electronic mail: miguel@dynamics.qf.ub.es; r.sayos@dynamics.qf.ub.es

saturated,[4,16] unsaturated,[17,18] cyclic[19] and aromatic[20] hydrocarbons, alcohols,[21] aldehydes,[22] and amines.[23] For all these reactions a low amount of OH rotational excitation has been found. This result has been interpreted as resulting from a direct reaction mode and a favored collinear O–H–C approach of the $O(^3P)$ atom to the C–H bond under attack. The reactivity of $O(^3P)$ with hydrocarbon clusters has also been examined,[24] and it has been found that for small cyclohexane clusters the OH product is suppressed.

Quasiclassical trajectory (QCT) calculations on London–Eyring–Polanyi–Sato (LEPS) triatomic model potential energy surfaces[25] have led to quite a satisfactory description of the experimental results (excitation function and OH vibrorotational distribution) obtained[16] for reactions of $O(^3P)$ with saturated hydrocarbons. Some of the results of that work[25] (direct reaction dynamics and favored collinear O–H–C attack) have also been considered, as indicated above, in more recent investigations to interpret the results obtained for reactions with other organic compounds. A good accord with experimental[16] and QCT[25] OH rotational distributions has been obtained in a vibrationally adiabatic distorted wave (VADW) approximate quantum mechanical calculation.[26] A LEPS modified tetratomic model has been used to describe the reaction of $O(^3P)$ with hydrocarbon–argon clusters.[27]

The main goal of this contribution is to characterize the ground potential energy surface (PES) of the $O(^3P)+CH_4 \rightarrow OH+CH_3$ reaction and to derive, as a first approximation, a triatomic analytical representation of the ground PES useful to study the kinetics and dynamics of this reaction. In this model the methyl group is treated as a single atom of mass equal to 15.0 a.m.u. placed in its center of mass. This modeling of the CH_3 group has been used previously with quite good results, see, e.g., Refs. 28 and 29. This work is organized as follows. Section II deals with the *ab initio* calculations and the fitting of the $OH(CH_3)$ ground PES. Section III shows the variational transition state theory (VTST) and QCT rate constant calculations, and also the QCT vibrorotational distribution of the OH product. In Sec. IV the concluding remarks are given.

II. POTENTIAL ENERGY SURFACE

A. *Ab initio* calculations

For C_1, C_s, and C_{3v} symmetries, the following PES correlate with the asymptotic regions of reaction (1): (a) reactants: $(3)\,^3A(C_1)$, $^3A'+(2)\,^3A''(C_s)$, $^3A_2+{}^3E(C_{3v})$; (b) products: $(2)\,^3A+(2)\,^1A(C_1)$, $^3A'+{}^3A''+{}^1A'+{}^1A''(C_s)$, $^3E+{}^1E(C_{3v})$. Hence, both asymptotes may correlate adiabatically under different symmetries through the following PES: $(2)\,^3A$ in C_1, $^3A'+{}^3A''$ in C_s, and ^3E in C_{3v}. The C_1 symmetry is the most relevant for theoretical studies on the dynamics of reactions that involves four or more atoms. Here, we have also taken into account higher symmetries since, as it will be shown below, the two O...H...CH_3 saddle points ($^3A'$ and $^3A''$) of reaction (1) have nearly identical C_s geometries which are very close to C_{3v} symmetry. As the $O(^3P)$ atom approaches the CH_4 molecule in C_{3v} symmetry (^3E PES), a Jahn–Teller conical intersection occurs.[30] A nontotally symmetric vibrational normal mode that shifts the $O(^3P)$ atom off the C–H axis splits the ^3E PES into the $^3A'$ and $^3A''$ PES. Although both PES are coupled by this vibrational mode, due to the approximations used in this work, this coupling has not been considered neither in the *ab initio* calculations nor to determine the partition functions along the reaction path and in the QCT calculations (Sec. III).

We have carried out an *ab initio* study mainly centered on the ground PES ($1^3A''$ in C_s) of reaction (1) by means of the GAUSSIAN 94 package of programs.[31] This has enabled us to characterize the stationary points and to calculate a number of points of the PES. After several checks, we have selected as a suitable calculation method the unrestricted second-order Møller–Plesset perturbation theory (UMP2) method using a large basis set [6-311G($3d2f$,$3p2d$), 172 basis functions], UMP2/6-311G($3d2f$,$3p2d$) *ab initio* level hereafter, to locate the stationary points and connections between them. All geometry optimizations have been carried out at this *ab initio* level. The energies of the set of *ab initio* points of the PES required to obtain, as a first approximation, a triatomic analytical representation suitable for dynamical studies, have been calculated at the spin projected unrestricted fourth-order Møller–Plesset perturbation theory (PUMP4) method using the same basis set, PUMP4/6-311G($3d2f$,$3p2d$) *ab initio* level hereafter. Each single point calculation at this level takes about 9 hours of c.p.u. time on a single processor of a Silicon Graphics O2000 workstation with 1 Gbyte of memory. The spin projected method has been employed to eliminate quite small spin contaminations ($2.01<\langle S^2\rangle/\hbar^2<2.05$) in the PES. The Møller–Plesset calculations have been performed in a standard way, i.e., including single, double, triple, and quadruple excitations, and all the electrons have been correlated. The stationary points [reactants, $^3A''$ and $^3A'$ transition states (saddle points), $^3A''$ products valley minimum and products] have been located and characterized (geometry, energy, and harmonic frequencies) using standard procedures (analytical gradients are available at the UMP2 level). In the next paragraphs the present *ab initio* results will be compared with experimental data and previous *ab initio* calculations.

The energetics of the system using different methods and basis sets is shown in Table I, considering the $O\cdots H\cdots CH_3$ $^3A''$ saddle point and asymptotes relevant to the triatomic model of reaction (1). For the best methods used here [UMP2/6-311G($3d2f$,$3p2d$) level for geometries and frequencies and PUMP4//UMP2/6-311G($3d2f$,$3p2d$) level for energies, including the UMP2 zero point energy (ZPE) when necessary] there is a good agreement with the experimental structures and frequencies of the CH_4, CH_3, OH, and CH_3O molecules (Table II), and the energetics of the $OH+CH_3$ and CH_3O+H reaction channels is also well described (Table I). The saddle point and products valley minimum structures are plotted in Fig. 1. Their properties are indicated in Tables III and IV, including also the properties of the $O\cdots H\cdots CH_3$ $^3A'$ saddle point.

The UMP2/6-311G($3d2f$,$3p2d$) calculations of this work show the existence of two nearly identical saddle points of C_s geometry ($^3A''$ and $^3A'$ electronic states) very close to C_{3v} symmetry with a PUMP2//UMP2 energy of,

TABLE I. Energetics of the system using different methods and basis sets.

Method	$E+$ZPE/kcal mol^{-1} [a,b]		
	$OHCH_3$ $^3A''$ saddle point	$OH+CH_3$	CH_3O+H
PUMP2//UMP2/6-311G($2df$,$2pd$)	11.9 (15.6)	2.5 (6.5)	14.4 (19.3)
PUMP2//UMP2/6-311G($3d2f$,$3p2d$)	9.4 (13.3)	−0.4 (3.6)	11.8 (16.7)
PUMP4//UMP2/6-311G($3d2f$,$3p2d$)	9.4 (13.3)	1.3 (5.3)	15.1 (20.0)
Experimental data	9.3, 10.0±1.2[c]	1.803[d]	14.2[e]

[a]Energy referred to reactants. The theoretical ZPE values correspond to the UMP2 data. The values in parentheses correspond to the energies without including the UMP2 zero point energies.
[b]Absolute values of energy (H) for $O(^3P)+CH_4$ are: −115.398 441 (UMP2/6-311G($2df$,$2pd$)), −115.400 018 (PUMP2//UMP2/6-311G($2df$,$2pd$)), −115.410 260 [UMP2/6-311G($3d2f$,$3p2d$)], −115.411 909 [PUMP2//UMP2/6-311G($3d2f$,$3p2d$)], and −115.456 209 [PUMP4//UMP2/6-311G($3d2f$,$3p2d$)].
[c]Experimental activation energy determined from the Arrhenius plot of the recommended rate constants (Ref. 6 and Refs. 5 and 7 respectively) in the 400–575 K temperature interval.
[d]$\Delta H^\circ_{0\,K}$ (Ref. 2).
[e]$\Delta H^\circ_{0\,K}$ (Refs. 2 and 32).

respectively, 13.3 and 13.4 kcal mol^{-1} above reactants (Table III). A single point calculation at the PUMP4//UMP2 level leads to the same energy for both stationary points. The $^3A'$ saddle point has, however, two imaginary frequencies, 2258.1i and 173.5i cm^{-1}, the lowest one corresponding to a bending of the O–H–C angle. We have been unable to determine a $^3A'$ saddle point with a single imaginary frequency. This situation has also been reported in Ref. 15. The inclusion of the zero point energy from the UMP2 frequencies (Table IV) leads to the $^3A''$ saddle point having an energy barrier of 9.4 kcal mol^{-1}. This value is consistent with the experimental activation energy [9.3 and 10.0 ±1.2 kcal mol^{-1} (cf. Table I)].

A minimum, also of C_s geometry ($^3A''$ electronic state) and very close to C_{3v} symmetry, has been located in the products valley (Table III). There is no charge transfer between the OH and CH_3 fragments of the minimum. The stabilization energy with respect to the $OH+CH_3$ products arises mainly from the interaction of the OH fragment electric dipole moment (nearly identical to that of OH) with the very small CH_3 fragment electric dipole moment placed

TABLE II. Properties of the reactants and products molecules.[a]

CH_4 $X^1A_1(T_d)$						
R_{CH}/Å	This work	1.083				
	Experimental[c]	1.0870_7				
ν/cm^{-1}	This work	1352.2 (T_2)	1585.8 (E)	3073.0 (A_1)	3213.6 (T_2)	
	Experimental[d]	1306.0	1534.0	2916.5	3018.7	
CH_3 $X^2A_2''(D_{3h})$						
R_{CH}/Å	This work	1.072				
	Experimental[c]	1.0767				
ν/cm^{-1}	This work	471.3 (A_2'')	1430.5 (E')	3177.4 (A_1')	3377.1 (E')	
	Experimental[d]	580	1383	3002	3184	
OH $X^2\Pi(C_{\infty v})$						
R_{OH}/Å	This work	0.960				
	Experimental[e]	0.96966				
ν/cm^{-1}	This work	3884.2 (Σ^+)				
	Experimental[e]	3737.76_1				
CH_3O $X^2A'(C_s)$[b]						
R_{CO},$R_{CH'}$,$R_{CH''}$/Å	This work	1.366	1.096	1.089		
	Experimental[f]	1.3637	1.0958	1.0958		
∠H′CO,∠H″CO/°	This work	105.1	112.9			
	Experimental[f]	111.27	111.27			
ν/cm^{-1}	This work	806.4 (A'')	970.7 (A')	1137.9 (A')	1412.4 (A')	1428.4 (A'')
		1538.7 (A')	3010.0 (A')	3093.2 (A')	3133.6 (A'')	

[a]See Fig. 1 for the internal coordinates definition.
[b]Experimental distances and angles between effective nuclear positions derived from isotopic differences in rotational constants (Ref. 36). The methoxy radical has a C_s structure close to C_{3v} symmetry due to the Jahn–Teller effect (see, e.g., Ref. 37).
[c]Reference 33.
[d]Reference 34.
[e]Reference 35.
[f]Reference 36.

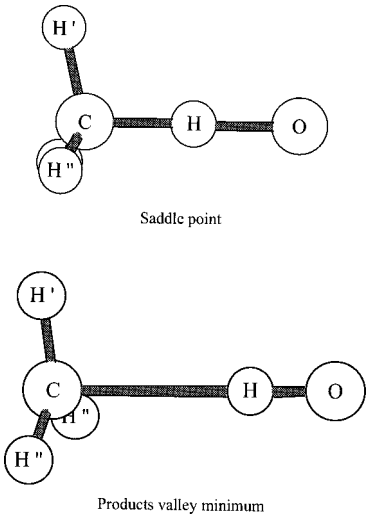

FIG. 1. $^3A''$ saddle point and products valley minimum structures.

along the C–H axis of the attacked bond (the CH_3 fragment is not completely planar) and also with the corresponding electric quadrupole moment (nearly identical to that of CH_3). The minimum is placed 2.3 and 2.6 kcal mol^{-1} below products at, respectively, the PUMP2//UMP2 and PUMP4//UMP2 levels. Once the basis set superposition error (BSSE) is included in the PUMP4//UMP2 calculation using the counterpoise method,[38] the minimum becomes placed 1.5 kcal mol^{-1} below products. However, if the ZPE is added to the energy values obtained after taking into account the BSSE, the minimum disappears, as it has an energy of 0.4 kcal mol^{-1} above the OH+CH_3 products.

Two saddle points ($^3A''$ and $^3A'$) almost identical in energy but differing slightly in the O–H–C bending angle have also been found in Ref. 15. The UMP2/cc-pVTZ geometries and the energy from scaled calculations (PUMP2-SAC//UMP2//cc-pVTZ) of Ref. 15 are very close to the values reported here (Table III). The UMP2 barrier is 17.84 kcal mol^{-1} while the scaled calculations lead to a value of 14.0 kcal mol^{-1}. After inclusion of the UMP2 ZPE for the $^3A''$ saddle point, the scaled calculations barrier becomes equal to 10.2 kcal mol^{-1},[15] a value consistent with the experimental activation energy [9.3 and 10.0$\pm$1.2 kcal mol^{-1} (cf. Table I)]. The Becke's 1988 functional (HFB, Hartree–Fock–Becke) with the 6-311G($2d$,$2p$) basis, the recommended method in Ref. 14, gives (without specifying the electronic state) a barrier height of 9.7 kcal mol^{-1} including ZPE.[14] This result is also consistent with the experimental activation energy. UMP2/6-31G(d,p) calculations[13] show the existence of two C_s saddle points ($^3A''$ and $^3A'$) almost identical in energy but differing slightly in geometry, as it has also been obtained in this work and in Ref. 15. The calculated PUMP4/6-31G(d,p)//UMP2/6-31G(d,p) barrier is equal to 15.3 kcal mol^{-1} (including UMP2 ZPE). This value is approximately 5 kcal mol^{-1} higher than the experimental activation energy, and the calculated difference in the barrier heights on the 1 $^3A''$ and 1 $^3A'$ PES (including UMP2 ZPE) is only 0.01 kcal mol^{-1} (spin projection at the PUMP4 level lowers the calculated barrier by 1.7 kcal mol^{-1}). POL-Cl (polarization configuration interaction) calculations[12] lead to a saddle point of C_{3v} symmetry (^3E electronic state). The calculated barrier height including ZPE was 10.2 kcal mol^{-1} using a [$3s2p1d/2s1p$] basis set, after an estimation of the basis set error taking into account the results obtained for the O(^3P)+H_2→OH+H system. For nonlinear O–H–C geometries, the ^3E PES splits into the 1 $^3A''$ and 1 $^3A'$ PES. The O–H–C bending curves for both surfaces are very close to each other and conventional transition state calculations treating the CH_3 group as a point mass lead to an

TABLE III. Properties of the saddle points and products valley minimum.[a]

Stationary point	R_{OH}/Å	R_{HC}/Å	$R_{H'C}$/Å	$R_{H''C}$/Å	∠CHO/°	∠H′CH/°	∠H″CH/°	∠H′CHO/°	E+ZPE/kcal mol^{-1}
Saddle point[b]									
This work $^3A''$	1.206	1.254	1.080	1.080	180.7	104.7	104.4	180.0	9.4 (13.3)
$^3A'$	1.206	1.254	1.080	1.080	179.4	104.3	104.6	0.0	(13.4)
Ref. 15 $^3A''$	1.201	1.250	1.076	1.076	180.8	104.6	104.1	180.0	10.2 (14.0)
$^3A'$	1.201	1.250	1.077	1.076	179.3	103.9	104.5	0.0	
Ref. 14[c]	1.198	1.396	1.102	1.102	180.4	103.3	103.3	180.0	9.7 (13.4)
Ref. 13 $^3A''$	1.179	1.289	1.081	1.081	182.1	104.9		180.0	15.3 (19.1)
$^3A'$	1.179	1.289	1.082	1.081	179.0	103.9		0.0	15.3 (19.1)
Ref. 12 ^3E	1.20	1.36	1.08	1.08	180.0	103.1	103.1		10.2 (12.0)
Experimental									9.3, 10.0$\pm$1.2[d]
Minimum[b]									
This work $^3A''$	0.966	2.234	1.074	1.073	180.6	93.5	92.5	180.0	0.6 (2.7)[e]

[a]See Fig. 1 for the internal coordinates definition. Energy referred to reactants and the values in parentheses correspond to the energies without including zero point energies.

[b]The *ab initio* methods are the following: this work: geometry, frequencies, and ZPE at the UMP2/6-311G($3d2f$,$3p2d$) level and energy (E) at the PUMP4//UMP2/6-311G($3d2f$,$3p2d$) level; Ref. 15: geometry, frequencies, and ZPE at the UMP2/cc-pVTZ level and energy (E) at the PUMP2-SAC//UMP2/cc-pVTZ level; Ref. 14: Becke's 88 (HFB) DFT/6-311G($2d$,$2p$); Ref. 13: geometry, frequencies, and ZPE at the UMP2/6-31G(d,p) level and energy (E) at the PUMP4/6-311G(d,p)//UMP2/6-31G(d,p); Ref. 12: POL-Cl/[$3s2p1d/2s1p$].

[c]Electronic state not indicated.

[d]Experimental activation energy determined from the Arrhenius plot of the recommended rate constants (Ref. 6 and Refs. 5 and 7 respectively), in the 400–575 K temperature interval.

[e]The energy with respect to the OH+CH_3 products is −0.7 (−2.6). If the BSSE is computed using the ''counterpoise'' method (Ref. 38), then the energetics of the minimum is 1.7 (3.8) kcal mol^{-1} with respect to reactants and 0.4 (−1.5) kcal mol^{-1} with respect to the OH+CH_3 products.

TABLE IV. Harmonic normal mode vibrational frequencies (cm^{-1}) for the $^3A''$ and $^3A'$ saddle points and the $^3A''$ products valley minimum.

Mode	$^3A''$ saddle point	$^3A'$ saddle point	$^3A''$ products valley minimum
ν_1	3276.0 (A')	3271.2 (A')	3752.6 (A')
ν_2	3231.3 (A'')	3232.0 (A'')	3368.8 (A'')
ν_3	3116.7 (A')	3116.2 (A')	3364.9 (A')
ν_4	1461.1 (A')	1466.8 (A')	3164.6 (A')
ν_5	1367.2 (A'')	1279.3 (A'')	1503.3 (A'')
ν_6	1239.9 (A')	1250.9 (A')	1431.1 (A')
ν_7	1139.4 (A')	1240.6 (A')	603.1 (A')
ν_8	1098.2 (A'')	1046.4 (A'')	405.4 (A'')
ν_9	624.4 (A')	624.8 (A')	403.2 (A')
ν_{10}	377.0 (A')	423.5 (A')	180.4 (A'')
ν_{11}	238.8 (A'')	2258.1i (A')	140.2 (A')
ν_{12}	2259.0i (A')	173.5i (A'')	128.6 (A')

estimated activation energy of 10 kcal mol^{-1}.[12] This value is also consistent with the experimental activation energy.

The saddle point geometries reported in the present work and previous studies[12–15] are very close to each other, with the exception of what happens for the C–H distance in the attacked bond, where differences up to 11% have been found (Table III). However, while in Ref. 12 a saddle point of C_{3v} symmetry with a linear O–H–C arrangement has been found, in the present work and in Refs. 13 and 15 two saddle points ($^3A''$ and $^3A'$) almost identical in energy but differing slightly in the O–H–C bending angle and the tilt of the methyl group have been located. In Ref. 14 only a saddle point has been reported without specification of the electronic state. The UMP2/6-311G($3d2f$,$3p2d$) frequencies obtained in our calculation (Table IV) are in general quite close to the UMP2/cc-pVTZ[15] and UMP2/6-31G(d,p)[13] ones. The UMP2/6-311G($3d2f$,$3p2d$) CH_3 geometry in the $O\cdots H\cdots CH_3$ saddle points resembles very much its geometry in the CH_4 molecule [$R_{CH}=1.0832$ Å, HCH angle $=109.5°$ (T_d)], and the C–H distance of the attacked bond and the O–H distance at the saddle points are, respectively, 0.1710 and 0.2457 Å higher than the corresponding equilibrium distances in the CH_4 and OH molecules. A nearly identical situation also occurs in Ref. 15. The UMP2/6-311G($3d2f$,$3p2d$) products valley minimum obtained here is very close to the $OH+CH_3$ asymptote. The CH_3 geometry at this point is not completely planar but is nearly identical to the geometry of the CH_3 radical [$R_{CH}=1.0720$ Å (D_{3h})]. The OH separation at the minimum is also nearly identical to the equilibrium distance in the OH molecule (0.9604 Å).

B. Analytical potential energy surface

To describe the ground PES ($1\,^3A''$ under C_s symmetry) for reaction (1), a triatomic model where the CH_3 radical is treated as a single atom (CH_3) of 15.0 a.m.u. placed in the center of mass of the radical has been considered. The same type of analytical expression (many-body expansion[39]) and programs[40,41] used in previous works of our group [e.g., $N(^4S)+NO$,[42] $O(^3P)+CS$,[43] $H(^2S)+Cl_2$ and $Cl(^2P)+HCl$,[44] and $N(^4S)+O_2$[45] reactions] have also been employed here. According to our approach, the analytical PES can be represented as follows:

$$V(R_1,R_2,R_3)=V^{(2)}_{OH}(R_1)+V^{(2)}_{H(CH3)}(R_2)+V^{(2)}_{O(CH3)}(R_3)+V^{(3)}_{OH(CH3)}(R_1,R_2,R_3), \quad (2)$$

where $V^{(2)}$ and $V^{(3)}$ are the two-body and three-body terms, respectively, and R_1,R_2,R_3 are the O–H, H–(CH_3), and O–(CH_3) distances, respectively.

The two-body terms (diatomic potential energy curves) have been fitted using the extended-Rydberg potential up to third order,

$$V^{(2)}(\rho)=-D_e(1+a_1\rho+a_2\rho^2+a_3\rho^3)e^{-a_1\rho}, \quad (3)$$

where D_e and R_e are the dissociation energy and equilibrium bond length of the corresponding diatomic or pseudodiatomic molecule, respectively, and ρ is defined as being equal to $R-R_e$. The optimal a_i diatomic parameters have been obtained for each molecule using a nonlinear least-squares procedure,[40] by fitting a set of nine diatomic or pseudodiatomic *ab initio* points calculated around the equilibrium distance (PUMP4//UMP2 level). For the X–(CH_3) species (X=H, O), the CH_3 *ab initio* geometry was optimized in all points of the X–(CH_3) pseudodiatomic curve. The extended-Rydberg function provides a very good fitting in all cases. The optimal diatomic parameters obtained in the fitting procedure are shown in Table V, and the spectroscopic constants derived from them for the OH, H(CH_3), and O(CH_3) molecules are given in Table VI.

The three-body term consists of a second-order polynomial expressed in terms of three internal coordinates

TABLE V. Optimal parameters for the analytical triatomic PES model.

Two-body terms:[a] Species	a_1/Å^{-1}	a_2/Å^{-2}	a_3/Å^{-3}
O–H	4.847 81	6.359 60	7.569 59
H–(CH_3)	2.849 45	0.455 54	1.449 76
O–(CH_3)	4.681 14	6.829 35	7.292 87

Three body term:[b]					
		c_{200}	2.650 66	γ_1	1.502 97
c_{000}	4.655 35				
		c_{110}	14.969 65		
				γ_2	1.169 20
c_{100}	−0.885 45				
		c_{101}	−6.723 54		
				γ_3	1.633 81
c_{010}	0.274 25				
		c_{020}	2.152 12		
				R^0_{OH}	1.2061
c_{001}	1.322 40				
		c_{011}	−4.587 66		
				$R^0_{H-(CH_3)}$	1.3086
		c_{002}	4.005 84		
				$R^0_{O-(CH_3)}$	2.5147

[a]The dissociation energies and equilibrium distances used in the fitting are given in Table VI.
[b]Units are: c_{ijk}/eV Å$^{-(i+j+k)}$, γ_i/Å^{-1}, R_i/Å.

TABLE VI. Properties of the diatomic and pseudodiatomic molecules.

Species	D_e/eV	R_e[a]/Å	ν_e/cm^{-1}	$\nu_e x_e$/cm^{-1}	B_e/cm^{-1}	α_e/cm^{-1}
O–H						
Analytical fit	4.6285	0.9604	3783.3	95.03	19.28	0.9557
Experimental[b]	4.621	0.969 66	3737.76_1	84.881_3	18.910_8	0.7242
H–(CH_3)						
Analytical fit	4.8605	1.1559	3176.1	81.15	13.35	0.5131
Experimental	4.820[c]	1.1562[d]				
O–(CH_3)						
Analytical fit	3.9916	1.4443	1075.4	6.400	1.043	0.1414×10^{-1}
Experimental	4.06[e]	1.4407[f]				

[a]Equilibrium distances for the pseudodiatomic H–(CH_3) and O–(CH_3) molecules correspond to the distances between the atom and the pseudoatom (CH_3) center of mass. See text.
[b]Reference 35.
[c]From D_0[H-(CH_3)] of Ref. 30 and taking into account the UMP2/6-311G($3d2f$,$3p2d$) frequencies calculated here for CH_4 and CH_3.
[d]Reference 33.
[e]Estimated from $\Delta H^0_{f,0\,\mathrm{K}}$ of CH_3O (Ref. 32), O(^3P), and CH_3 (Ref. 2), assuming D_0 approximately equal to $\Delta H^0_{f,0\,\mathrm{K}}$ and taking into account the UMP2/6-311G($3d2f$,$3p2d$) frequencies calculated here for CH_3O and CH_3.
[f]R_s, distance between effective nuclear positions derived from isotopic differences in rotational constants (Ref. 36).

(ρ_1,ρ_2,ρ_3), defined as $\rho_i = R_i - R_i{}^0$, where the selected reference structure ($R_1{}^0, R_2{}^0, R_3{}^0$) matches the geometry of the triatomic collinear saddle point ($R_1{}^0 = 1.2061$, $R_2{}^0 = 1.3086$, $R_3{}^0 = 2.5147$ Å), and a range function $T(\rho_1,\rho_2,\rho_3)$. This function cancels the three-body term as one of the three atoms is separated from the other two,

$$V^{(3)}{}_{\mathrm{OH(CH3)}}(\rho_1,\rho_2,\rho_3) = P(\rho_1,\rho_2,\rho_3)T(\rho_1,\rho_2,\rho_3), \quad (4)$$

where

$$P(\rho_1,\rho_2,\rho_3) = \sum_{i,j,k=0}^{0\leq i+j+k\leq 2} c_{ijk}\rho_1^i\rho_2^j\rho_3^k, \quad (5)$$

with i, j, and k positive integer numbers, and

$$T(\rho_1,\rho_2,\rho_3) = \prod_{i=1}^{3}\left[1-\tanh\left(\frac{\gamma_i\rho_i}{2}\right)\right]. \quad (6)$$

The ten linear parameters ($\{c_{ijk}\}$ polynomial coefficients) and three nonlinear ones ($\{\gamma_i\}$ range function parameters) of the three-body term have been determined by a weighted nonlinear least-squares procedure,[41] using the *ab initio* saddle point and 34 additional points concentrated mainly along the O+H–(CH_3) minimum energy path (20 points), which is essentially collinear (179–180°), and the saddle point bending energy curve (7 points). In the fitting, a weight of 1.0 was used for each one of these points and for the first partial derivatives of the energy (equal to zero) with respect to, respectively, R_{OH}, $R_{\mathrm{H(CH3)}}$ and the O–H–(CH_3) angle at the saddle point geometry. Moreover, four points corresponding to the O(^3P) approach on the (CH_3) side (weight = 0.01) and three points with O–H–(CH_3) angles of about 100° (weight = 0.1) were also considered. As previously indicated, the geometry optimizations required (saddle point and minimum energy path) were performed at the UMP2 level, while the energies were in all cases PUMP4 values. The optimal three-body parameters and the properties of the saddle point and products valley minimum of the analytical PES are given in Tables V and VII, respectively. There is a good agreement between the *ab initio* properties of the stationary points and those resulting from the fitting. For the 28 *ab initio* points with weight = 1.0, the root-mean-square deviation (RMSD) is equal to 0.0205 eV (0.47 kcal mol^{-1}), while for the full set of 35 points the RMSD is 0.1396 eV (3.22 kcal mol^{-1}). The saddle point properties fitted (geometry and energy) are in good accord with the *ab initio* calculations with average differences of 0.6%. The frequencies are also equally well described with the exception of the symmetric stretching. Even though it was not treated as a stationary point in the fitting procedure (inclusion of the

TABLE VII. Properties of the saddle point and products valley minimum of the analytical triatomic PES model.

Stationary point	$R_{\mathrm{O-H}}$/Å	$R_{\mathrm{H-(CH_3)}}$/Å	∠O–H–(CH_3)/°	E/kcal mol^{-1} [a]	E + ZPE/kcal mol^{-1} [a]	ν_i/cm^{-1}
Saddle point[b,c]	1.2004	1.3135	180.0	13.1	11.2	1496.5i (Σ^+), 607.0 (Σ^+), 605.1 (Π)
Minimum[c]	0.9402	2.3636	180.0	2.1	4.0	3896.8 (Σ^+), 119.9 (Σ^+), 254.1 (Π)

[a]Energy referred to reactants. The energy (E) of the minimum with respect to OH+CH_3 products is −3.2 kcal mol^{-1} (−2.1 kcal mol^{-1} taking into account the ZPE).
[b]*Ab initio* pseudotriatomic frequencies (cm^{-1}): 1610.6i (Σ^+), 341.0 (Σ^+), 603.0 (Π).
[c]Both the saddle point and products valley minimum of the analytical triatomic PES model present a collinear ($C_{\infty v}$) O–H–(CH_3) configuration instead of the quasicollinear (C_s) O–H–C configuration obtained at the *ab initio* level.

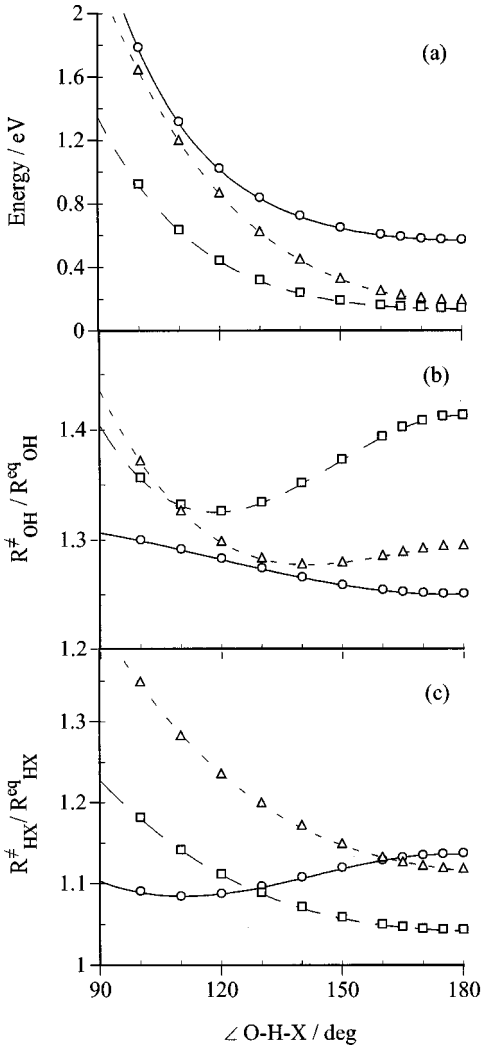

FIG. 2. Angular dependence vs O–H–X attack angle [X=(CH_3), (R), Br] of the (a) barrier height and (b), (c) geometry (see text) for the ground PES of reactions O(^3P)+H–(CH_3), this work (''○''), O(^3P)+H-(R) (tertiary C–H bond), Ref. 24 (''△''), and O(^3P)+HBr, Ref. 44 (''□''). Energy is given relative to reactants.

first partial derivatives as equal to zero), the products valley minimum is also quite well described, falling only 0.6 kcal mol^{-1} below the *ab initio* one.

In spite of the good agreement that exists between the analytical PES and the *ab initio* calculations, once the original geometries have been transformed into pseudotriatomics, when the ZPE is included the accord between the different energies involved is not so good, because the ZPE of CH_4 and CH_3 are not properly taken into account. Thus, e.g., the barrier and endoergicity are respectively equal to 11.2 and 6.2 kcal mol^{-1} for the analytical PES, and 9.4 and 1.3 kcal mol^{-1} for the PUMP4//UMP2 *ab initio* calculation. On the other hand, the saddle point imaginary frequency of the analytical PES (1496.5*i* cm^{-1}), which is related to the tunneling probability through the corresponding barrier, is 66.2% the UMP2 *ab initio* one (2259.0*i* cm^{-1}). These problems result from the simplicity of the triatomic model and some consequences of them can be seen in the rate constant calculation (Sec. III A).

In Fig. 2 the dependence of the barrier height relative to reactants with respect to the O–H–(CH_3) attack angle is shown, together with the corresponding dependences for previously reported LEPS empirical PES for the O(^3P)+H–(R)→OH+(R)[25] (triatomic model with H–(R) simulating a tertiary C–H bond) and O(^3P)+HBr→OH+Br[46] related reactions. All the PES have a collinear saddle point with the O(^3P)+H–(CH_3) system presenting the largest barrier. The barrier height versus attack angle dependence for the reaction with H–(CH_3) is nearly parallel to that for HBr. However, the barrier for H–(R) rises more sharply as the attack angle decreases. The ratio of distances $R^{\neq}_{OH}/R^{eq}_{OH}$ and $R^{\neq}_{HX}/R^{eq}_{HX}$ vs the O–H–X attack angle [X=(CH_3), (R), Br] are also shown in Fig. 2, where $R^{\neq}$ and R^{eq} are, respectively, the equilibrium distances at the barrier and in the corresponding diatomic or pseudodiatomic molecule. The ratios of the O(^3P)+HBr PES clearly reflect the existence of a barrier lying closer to reactants than in the case of the other two systems. The implications of these facts on the dynamics will be analyzed in Sec. III B.

III. KINETICS AND DYNAMICS

A. Thermal rate constant

The thermal rate constant for reaction (1) has been calculated within the 300–2500 K temperature range at different levels of the conventional (TST) and variational (VTST) transition state theories[47] using the POLYRATE program;[48] see also, e.g., Refs. 43–45. The following levels of TST and VTST have been considered: TST, CVT, and ICVT, and for each level two types of tunneling corrections have been taken into account: SCT and LCT. The acronyms CVT and ICVT correspond, respectively, to the canonical and improved canonical VTST, and SCT and LCT to the small and large curvature types of tunneling corrections. The methods used to treat the different cases of minimum energy curvature are the standard ones included in the POLYRATE program.[48] The centrifugal dominant small curvature semiclassical adiabatic ground state (CD-SCSAG) method and the large curvature ground state version 3 (LCG3) method have been used, respectively, for the SCT and LCT cases. The microcanonical optimized multidimensional tunneling (μOMT) correction has also been considered, the ICVT/μOMT method being the highest level of VTST calculations used. However, it was not possible to employ it when, instead of the analytical PES, the *ab initio* saddle point and a set of points along the intrinsic reaction coordinate (IRC) were considered to treat explicitly all atoms of the system. This was due to the fact that the number of points along the IRC required to do this is much larger than the number of points available (six points between the saddle point and reactants and also between the saddle point and products). The QCT method[49–51] as implemented in the TRIQCT program[52] has been employed to calculate the rate constant at 1500, 2000, and 2500 K. The accuracy of the numerical integration of Hamilton's differential equations has been verified by checking the conservation of total energy and angular momentum along every trajectory, and performing back-integrations on samplings of trajectories. An initial distance of 10 Å between the O(^3P) and the H–(CH_3) center of

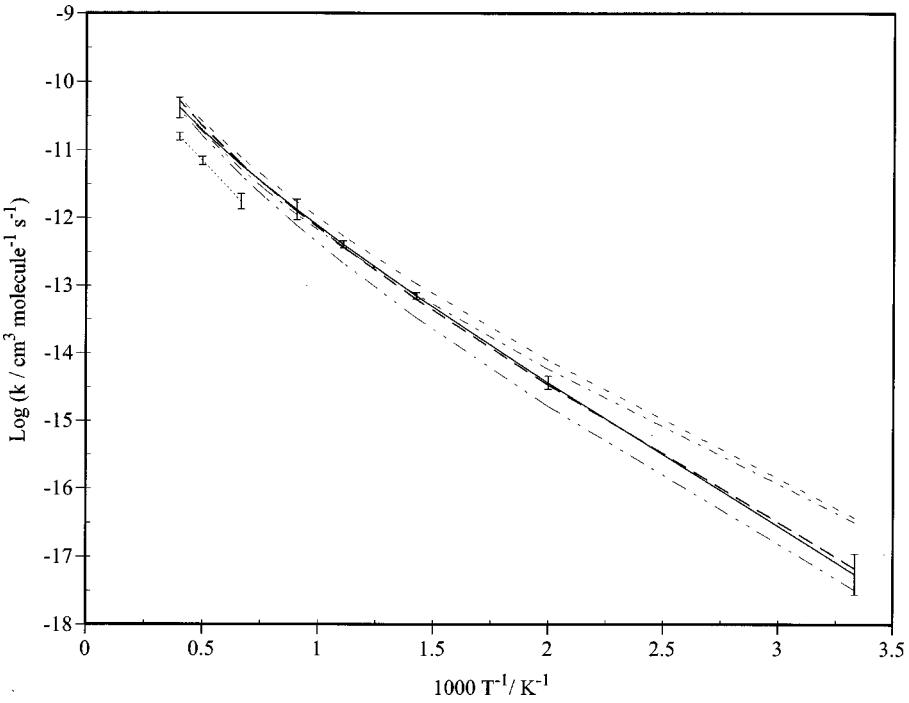

FIG. 3. Arrhenius plot of the rate constant: recommended experimental data (Refs. 5 and 7) (''____''), recommended experimental data (Ref. 6) (''— — —''), *ab initio* ICVT/SCT data (''- - - -''), analytical PES ICVT/μOMT (''—- — -''), analytical PES ICVT/SCT (''–---–''), and analytical PES QCT (''.....''). QCT error bars correspond to one standard deviation.

mass has been used. At this distance the reactants interaction energy can be neglected with respect to the reactants available energy. For each temperature, both E_T and the vibrorotational levels of the H–(CH_3) molecule have been sampled[50] according to the Maxwell–Boltzmann distribution.

From the electronic correlation between reactants and products (cf. Sec. II A), neglecting the possibility of nonadiabatic coupling between the two lowest PES, it comes out that the rate constant for reaction (1) can be expressed as

$$k=\frac{3k(1\,^3A)+3k(2\,^3A)}{5+3e^{-E(^3P_1)/RT}+e^{-E(^3P_0)/RT}} \quad \text{(under } C_1 \text{ symmetry)} \tag{7}$$

or

$$k=\frac{3k(1\,^3A'')+3k(1\,^3A')}{5+3e^{-E(^3P_1)/RT}+e^{-E(^3P_0)/RT}} \quad \text{(under } C_s \text{ symmetry)}, \tag{8}$$

where $E(^3P_1)$ and $E(^3P_0)$ are, respectively, the energies of the $^3P_1$ and $^3P_0$ levels of O(^3P), 158.29 and 226.99 cm^{-1},[53] relative to the ground level ($^3P_2$). The spin-orbit splittings must be included, as they are only negligible at high temperatures. Considering, e.g., C_s symmetry, since the $1\,^3A''$ and $1\,^3A'$ saddle points belong to this symmetry, the contribution of the first excited $^3A'$ PES ($2\,^3A'$) to the rate constant is taken as zero, since this PES does not correlate adiabatically reactants and products and we have neglected nonadiabatic effects. Taking into account our results and previous works,[12,13,15] which show that both the $1\,^3A''$ and $1\,^3A'$ saddle points are nearly identical in geometry, energy, and frequencies, and their bending energy curves are quite close to each other (energy separation lower than 1.5 kcal mol^{-1} [12,15]) up to $\pm 30°$ away from the O–H–(CH_3) collinear saddle point structure, in this calculation we have assumed it reasonable to consider that both the $1\,^3A''$ and $1\,^3A'$ PES exhibit the same reactivity. This assumption leads to a plausible estimate of the reaction rate constant taking $k(2\,^3A)$ equal to $k(1\,^3A)$ or $k(1\,^3A')$ equal to $k(1\,^3A'')$ under, respectively, C_1 [Eq. (7)] or C_s [Eq. (8)] symmetries. To take into consideration that there are four equivalent hydrogen atoms in the methane molecule, assuming that the reaction channel involving each hydrogen atom is independent from the remaining ones, the TST, VTST, and QCT rate constants derived from the ground PES must be multiplied by four (statistical factor). In all transition state calculations, the rotational symmetry numbers have been omitted. The *ab initio* ICVT/SCT, triatomic (analytical PES) ICVT/SCT, ICVT/μOMT, and QCT, and recommended experimental[5–7] rate constant values are shown in Fig. 3 and Table VIII.

An experimental recommended expression for k over the 300–2500 K temperature range has been reported:[5,7] $k\,(\text{cm}^3\,\text{molecule}^{-1}\,\text{s}^{-1}) = 1.15\,10^{-15}\,T^{1.56}\exp(-4270/T)$. Within the 400–2000 K interval there is an excellent agreement between a number of reliable experimental determinations of the rate constant.[5,7] Nevertheless, at temperatures lower than 400 K, the value of k is considerably more unreliable, due to uncertainties in the reation stoichiometry. Another recommended expression for k[6] [$k(\text{cm}^3\,\text{molecule}^{-1}\,\text{s}^{-1}) = 2.2591\,10^{-12}(T/298)^{2.2}\exp(-3820/T)$] is in agreement with the former recommended expression, taking into account the experimental error margins. More recent experimental results at 1345–1840 K[8] and 980–1522 K[10] are also in accord with the recommended data.

The k(*ab initio*; ICVT/SCT) values are always higher than the experimental (exp.) ones,[5–7] although between 2500 and 1000 K the theoretical results fall in general within error margins with respect to measured data. The deviations become particularly significant at the lowest temperature considered (300 K), where k(*ab initio*; ICVT/SCT)/k(exp.)

TABLE VIII. Theoretical and experimental rate constants ($cm^3\,molecule^{-1}\,s^{-1}$).[a]

	Ab initio		Analytical PES				Experimental values	
T/K	ICVT	ICVT/SCT	ICVT	ICVT/SCT	ICVT/μOMT	QCT[b]	[c]	[d]
2500	5.55×10^{-11}	5.80×10^{-11} (4.3)	3.75×10^{-11}	3.90×10^{-11} (3.8)	4.22×10^{-11} (11.2)	$(1.57\pm0.20)\times10^{-11}$	5.28×10^{-11}	$(4.17\pm1.44)\times10^{-11}$
2000	2.41×10^{-11}	2.58×10^{-11} (6.7)	1.50×10^{-11}	1.59×10^{-11} (5.9)	1.80×10^{-11} (16.8)	$(6.87\pm0.98)\times10^{-12}$	2.21×10^{-11}	$(1.92\pm0.66)\times10^{-11}$
1500	6.90×10^{-12}	7.79×10^{-12} (11.4)	3.79×10^{-12}	4.21×10^{-12} (10.2)	5.21×10^{-12} (27.3)	$(1.72\pm0.46)\times10^{-12}$	6.20×10^{-12}	$(6.01\pm2.08)\times10^{-12}$
1300	3.40×10^{-12}	3.99×10^{-12} (14.9)	1.73×10^{-12}	2.00×10^{-12} (13.2)	2.63×10^{-12} (34.1)		3.06×10^{-12}	$(3.10\pm1.07)\times10^{-12}$
1100	1.36×10^{-12}	1.70×10^{-12} (19.7)	6.30×10^{-13}	7.67×10^{-13} (17.9)	1.11×10^{-12} (43.3)		1.24×10^{-12}	$(1.32\pm0.46)\times10^{-12}$
900	3.91×10^{-13}	5.43×10^{-13} (28.0)	1.59×10^{-13}	2.13×10^{-13} (25.2)	3.59×10^{-13} (55.7)		3.69×10^{-13}	$(4.06\pm0.47)\times10^{-13}$
700	6.29×10^{-14}	1.06×10^{-13} (40.9)	2.09×10^{-14}	3.34×10^{-14} (37.5)	7.29×10^{-14} (71.4)		6.31×10^{-14}	$(7.08\pm0.82)\times10^{-14}$
500	2.95×10^{-15}	7.84×10^{-15} (62.4)	6.84×10^{-16}	1.65×10^{-15} (58.6)	5.81×10^{-15} (88.2)		3.39×10^{-15}	$(3.65\pm0.84)\times10^{-15}$
300	3.40×10^{-18}	3.70×10^{-17} (90.8)	3.74×10^{-19}	3.26×10^{-18} (88.5)	3.20×10^{-17} (98.8)		6.77×10^{-18}	$(5.54\pm3.83)\times10^{-18}$

[a]The theoretical rate constant values shown here correspond to the ones derived from Eq. (7) (see also the text). For the VTST data, the values in parentheses correspond to the contribution of tunneling effect to the rate constant, expressed in percentage, i.e., 100 times the ratio $(k(\text{ICVT/SCT})-k(\text{ICVT}))/k(\text{ICVT/SCT})$ and equivalently for ICVT/μOMT.
[b]QCT errors correspond to one standard deviation.
[c]See Ref. 6.
[d]See Refs. 5 and 7.

$=5.5-6.7$. By contrast, for the analytical PES the ICVT/SCT method leads always to rate constant values lower than the experimental results. The $k(\text{analytical PES,ICVT/SCT})/k(\text{exp.})$ ratio is 0.5–0.6 between 300 and 1100 K, even though above 1300 K, agreement with measured data is reached when experimental errors are considered. The k(analytical PES; ICVT/μOMT) values are placed between k(analytical PES; ICVT/SCT) and k(*ab initio*; ICVT/SCT), being closer to the *ab initio* ICVT/SCT ones at 700 K and below. k(analytical PES; ICVT/μOMT) is in agreement with experimental data between 2500 and 700 K if experimental errors are included, and $k(\text{analytical PES; ICVT/}\mu\text{OMT})/k(\text{exp.}) = 4.7-5.8$ at 300 K.

At the same level of calculation the analytical PES leads to lower rate constant values than the method directly based on *ab initio* points, where all atoms are considered. This is due to the higher barrier that presents the analytical PES model after inclusion of the ZPE (cf. Sec. II B.). On the other hand, the fact that the best VTST method (ICVT/μOMT) leads to higher rate constant values than the ICVT/SCT method suggests that the overestimation of the rate constant from the *ab initio* ICVT/SCT method will be increased in an *ab initio* ICVT/μOMT calculation. This in turn could mean that higher level *ab initio* calculations would be needed to deal with reaction (1). However, at this point it is worth taking into consideration the best rate constant values reported in the dual level direct dynamics calculation of Ref. 15, which are in good agreement with experiments[5–7] within the full temperature interval (300–2500 K). These results were obtained using as a higher level *ab initio* calculations of similar quality as the one considered here (UMP2/cc-pVTZ, see also Sec. II A). These facts suggest that in respect to the calculation of the rate constant for reaction (1), the agreement between theory and experiment is probably more connected with the method used to derive the rate constant than with the accuracy of the high level *ab initio* calculations performed. In general, for this light atom transfer reaction it appears to be particularly difficult to describe the rate constant below 700 K, when tunneling has a very important or dominant contribution (38%–99%, cf. Table VIII) to reactivity.

The ICVT/SCT rate constant for the reverse reaction is much higher for the analytical PES than for the *ab initio* PES. The $k(\text{analytical PES})/k(ab\ initio\ \text{PES})$ ratio ranges from 27.0 to 141.7 between 2500 and 300 K, respectively. This is due to the errors in the ZPE correction in the context of the triatomic model, which become particularly important for the reverse reaction. Thus, the barrier including ZPE for the $OH+CH_3$ reaction is substantially lower for the analytical PES (5.0 kcal mol^{-1}) than in the case of the *ab initio* PES (8.1 kcal mol^{-1}).

QCT calculations have only been performed at 1500, 2000, and 2500 K due to the very small reactivity of this system. The reaction probability is equal to 0.25%, 0.71%, and 1.33%, respectively, for 1500, 2000, and 2500 K. About 90 000 trajectories have been calculated for each temperature. The maximum impact parameter (b_{max}) takes the following values: 1.948, 2.185, and 2.295 Å, respectively, for 1500, 2000, and 2500 K. k(analytical PES;QCT) is about one-third of k(exp.) and one-half of $k(\text{analytical PES; ICVT})$.

Even though the Arrhenius plot of the rate constant shows a large curvature (Fig. 3), additional insight into the differences between theoretical and experimental rate con-

TABLE IX. Arrhenius parameters for the 400–575 K temperature interval.

Method	E_a /kcal mol^{-1}	log(A/cm^3 molecule^{-1} s^{-1})
Ab initio, ICVT/SCT	8.66	−10.31
Analytical SEP, ICVT/μOMT	8.65	−10.60
Analytical SEP, ICVT/SCT	9.90	−10.44
Experimental[a]	9.27	−10.40
Experimental[b]	9.95± 1.22	−10.08± 0.79

[a]Reference 6.
[b]References 5 and 7.

stant values can be obtained comparing the Arrhenius parameters [activation energy (E_a) and preexponential factor (A)] within a temperature interval with a good linear relation between $\log k$ and $1/T$. Thus, for the 400–575 K range we have (Table IX): E_a(*ab initio*; ICVT/SCT) is equal to E_a(analytical PES; ICVT/μOMT) with E_a(analytical PES; ICVT/μ/OMT)/E_a(exp)=0.87–0.93 and E_a(analytical PES; ICVT/SCT)/E_a(exp.)=0.99–1.07; while $\log A$(theoretical)/$\log A$(exp.) is very close to one (0.99–1.05).

The imaginary frequency of the analytical PES is 66.2%, that of the *ab initio* PES (cf. Sec. II B). According to the simple expression of Wigner for the rate constant (k) correction due to tunneling,

$$\Gamma = 1 + \frac{1}{24}\left[\frac{h|\nu_{\text{imag}}|}{k_B T}\right]^2, \tag{9}$$

where $|\nu_{\text{imag}}|$ is the modulus of the imaginary frequency and k corrected is equal to the Γ k product, for the *ab initio* PES and T:900–2500 K tunneling contributes about twice as much to reactivity than in the case of the analytical PES. This ratio of tunneling contributions diminishes as temperature decreases, becoming 1.46 and 1.22 times at 500 and 300 K, respectively. These differences, however, become much smaller when more sophisticated treatments of tunneling are employed, as it will be shown below. This is due to the tunneling paths which are different and counterbalance the influence of the imaginary frequency.

The VTST relative contribution (in percentage) of tunneling to the rate constant defined as equal to 100 times the ratio [k(with tunneling)−k(without tunneling)]/k(with tunneling) is also given in Table VIII. The results obtained for (*ab initio*; ICVT/SCT) are very similar to those of (analytical PES; ICVT/SCT). From 2500 to 1500 K the relative contribution of tunneling increases from 4% to 11% and reaches values of 39% and 90%, respectively, at 700 and 300 K. The results obtained for (analytical PES; ICVT/μOMT) show quite a more important tunneling contribution than in previous cases over the temperature interval investigated (300–2500 K). Thus, from 2500 to 1500 K the tunneling contribution increases from 11% to 27%, reaching values of 71% and 99%, respectively, for 700 and 300 K. As expected, in all cases the relevance of tunneling increases as temperature decreases, because a progressively minor fraction of the reactants have energies above the barrier.

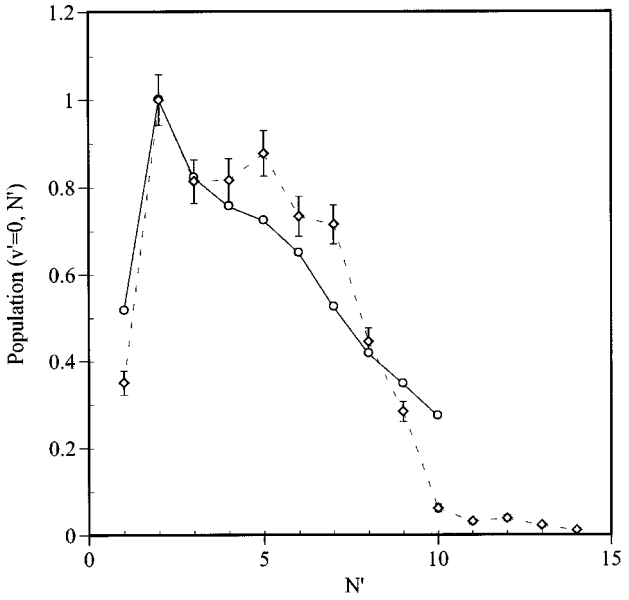

FIG. 4. OH($v'=0$) rotational distribution in terms of the N' quantum number (see text): experimental (Ref. 4) (“○”) and QCT (“◇”) results. QCT error bars indicate one standard deviation.

B. Vibrorotational distribution and microscopic reaction mechanism

The experimental nascent rotational distribution for OH($X\,^2\Pi_{3/2}, v'=0$) arising from reaction (1) with thermal CH_4 and translationally hot O(^3P) atoms, generated by laser photolysis of NO_2 at 248 nm, have been measured[4] (Fig. 4) using LIF detection of OH. No OH($v'=1$) molecules were detectable. From the experimental vibrational distribution of NO produced in the NO_2 photodissociation at 248 nm and the average rotational energy for each populated NO vibrational level (v:0–8),[54] we have determined the experimental relative translation energy distribution for the resulting O(^3P) hot atom using well-known procedures (see, e.g., Ref. 55). Taking into consideration the E_T values that lead to an energy content high enough to make possible the reaction of O(^3P) with thermal (298 K) H-(CH_3) molecules (E_T = 0.65, 0.55, and 0.50 eV with, respectively, relative populations of 1.000:0.154:0.154), we have carried out QCT calculations on reaction (1), running about 60 000 trajectories for each initial condition. In Fig. 4 it can be seen that quite a good agreement exists between the results of the QCT calculation and the experimental OH($v'=0$) rotational distribution. As the QCT method does not include the OH($X\,^2\Pi$) orbital ($\Lambda=1$) and spin ($S=1/2$) electronic angular momenta, we have assumed the total angular momentum quantum number (excluding the electronic and nuclear spins) of the OH molecule, N', as being equal to the rotational angular momentum quantum number (j') plus one. The first excited OH vibrational level, which was not detected in the experiments[4] (although this was not pursued systematically) shows very small populations for all these E_T values. The QCT $P(v'=0)/P(v'=1)$ ratio of populations is equal to 66.7, 25.0, and 12.3 for E_T= 0.50, 0.55, and 0.65 eV, respectively. This result is consistent with the experimental data.[4] On the other hand, only about 10% of reactive trajectories

lead to OH molecules with internal energy lower than the ZPE. If these reactive trajectories are removed from the statistics, the resulting vibrorotational distributions obtained are essentially identical to the ones originally reported.

The minimal available energy in products above ZPE ($E_{\text{barrier}}+\text{ZPE}_{\text{barrier}}-E_{\text{products}}-\text{ZPE}_{\text{products}}$) from the *ab initio* data (8.1 kcal mol^{-1}) is quite a bit larger than that obtained from the analytical PES (5.0 kcal mol^{-1}). This is due to the inadequacy of the triatomic model to deal with ZPE of polyatomic species (cf. Sec. II B). However, it has been shown that the OH internal energy distribution at collision energies a little above the barrier including ZPE is well described by the QCT method using the analytical PES. The 3.1 kcal mol^{-1} of difference between both available energies can be compared to the experimental average excitation vibrational energy found in the umbrella mode of CH_3 (1.51 kcal mol^{-1}),[3] resulting from reaction (1) with translationally hot O(^3P) atoms generated by laser photolysis of SO_2 at 193 nm. Although this vibrational mode is probably the most suited one to be excited by collisions with O(^3P), additional excitation in the remaining modes and also in the rotational levels could account for the energy difference. The above-mentioned facts indicate that the triatomic model proposed is able to describe the internal OH energy content and suggest that it could also be reasonable to deal with the translational energy distribution.

The reaction cross section (σ) for O(^3P) + H-(CH_3) (298 K) is quite small (0.04–0.23 Å^2) and increases with E_T, as expected for reactions with a barrier. The increase of σ is due to both increases in the reaction probability (0.8%–2.8%) and $b_{\max}$ (1.19–1.62 Å). The average fraction of energy appearing in products as relative translation ($\langle f'_T\rangle = 0.31-0.46$), vibration ($\langle f'_V\rangle = 0.62-0.46$), and rotation ($\langle f'_R\rangle = 0.07-0.08$) shows a small amount of energy released as OH rotation. As reactants E_T increases, however, the energy tends to appear preferably as relative translational energy of products. A $\mathbf{l}\rightarrow\mathbf{l}'$ angular momentum transformation trend has been observed, with $\mathbf{l}(\mathbf{l}')$ being the reactants (products) orbital angular momentum, according to what can be expected for a reaction with $\mathbf{H}-\mathbf{L}-\mathbf{H}$ kinematics. Regarding the average properties that involve two vectors it comes out that the angular distribution is clearly backward ($f/b = 0.014-0.163$), with the initial ($\mathbf{k}$) and final ($\mathbf{k}'$) relative velocity vectors forming an average angle of 132.0–119.7°, and, as expected, tends to be more forward as E_T increases. The OH rotational angular momentum ($\mathbf{j}'$) tends to be perpendicular to both $\mathbf{k}$ and $\mathbf{k}'$, with symmetrical distributions around 90°. The $\mathbf{l}'\mathbf{j}'$ distribution is very broad and relatively symmetrical around 90°, even though both vectors tend to become antiparallel as E_T increases.

The cold OH rotational excitation found [$\langle E_R\rangle = 0.058$ eV for OH($v'=0$), this work, and 0.072 eV for OH($X\,^2\Pi_{3/2}, v=0$), experimental[4]], both values are in agreement if errors are included] can be justified, in principle, on the basis of a preferred O–H–C collinear attack of the O(^3P) atom to the H–C bond to be broken. This interpretation has been invoked in previous studies of analogous O(^3P) reactions with hydrocarbons[4,16–20] and other organic compounds.[21–23] A deeper consideration on the origin of the low OH rotational excitation found will be given below.

The microscopic reactions mechanism has been studied for O(^3P) + H–(CH_3) ($T=298$ K) and $E_T=0.65$ eV, the most relevant initial condition explored, by analyzing the geometry and the PES energy distributions of the O–H–(CH_3) system in the strong interaction region. This region corresponds to the most representative minimum distance [$R_{\min}$(O–H(CH_3)] of the O(^3P) atom to the H–(CH_3) center of mass: $2.3<R_{\min}(\text{O–H}(\text{CH}_3))(\text{Å})<2.4$. A total amount of 88.1% of reactive trajectories reach this $R_{\min}$[O–H(CH_3)] interval and evolve further to progressively higher R[O–H(CH_3)] values, leading, finally, to products. These values are quite close to the O–H(CH_3) distance (2.43 Å) at the saddle point. Only 2.4% of reactive trajectories reach $R_{\min}[\text{O–H}(\text{CH}_3)]=2.3$ Å. Moreover, plots of samplings of reactive trajectories reveal that reaction (1) occurs through a direct reaction mode, with an average duration of 0.58 ps and a full width at half maximum (FWHM) time distribution of 0.25 ps.

The examination of the properties of reactive trajectories for $R[\text{O–H}(\text{CH}_3)]=2.4$ Å shows that the average O–H and H–(CH_3) distances, O–H–(CH_3) angle, and PES energy are, respectively, 1.42 (0.46)Å, 1.19 (0.32) Å, 146.2 (44.7)°, and 0.61 (0.20) eV above reactants (where the FWHM of each distribution is given in parentheses). The most remarkable result occurs for the O–H–(CH_3) angle which deviates substantially from collinearity (180°), although the collinear approach presents the lowest barrier to reaction. The analysis of the products energy distribution dependence on the O–H–(CH_3) angle at $R[\text{O–H}(\text{CH}_3)]=2.4$ Å reveals that $\langle f'_T\rangle$, $\langle f'_V\rangle$, and $\langle f'_R\rangle$ are essentially independent of this angle. For the 180–160, 160–140, and 140–120° intervals, respectively, the following average fractions of energy are obtained: $\langle f'_T\rangle = 0.45$, 0.45, and 0.43; $\langle f'_V\rangle = 0.45$, 0.48, and 0.49; $\langle f'_R\rangle = 0.07$, 0.05, and 0.06. The vibrorotational distributions exhibit similar shapes for all angular intervals.

To study the effect of the PES on the OH internal energy distribution, it is worth considering together the reactions of O(^3P) with H–(CH_3), HBr,[56] and H–(R)[25] [H–(R) models a primary, secondary, or tertiary C–H bond]. The OH product vibrational energy available increases as exothermicity increases, and this tendency correlates with the resulting decline of the barrier and its shift toward the reactants region. The rotationally cold OH distribution obtained for reactions of O(^3P) with organic compounds, as indicated before, has been interpreted as due to the presence of a collinear saddle point on the PES. However, the explanation is not so simple. Thus, for instance, the O(^3P) + HBr (300 K) reaction, which has been modeled using a LEPS PES (collinear saddle point), presents a substantial OH rotational excitation ($\langle f'_T\rangle = 0.26$, $\langle f'_V\rangle = 0.52$, and $\langle f'_R\rangle = 0.22$ for $E_T = 3.59-5.98$ kcal mol^{-1}).[56] This behavior can be more adequately interpreted on the basis of the barrier height dependence on the O–H–X attack angle (Fig. 2). Although the reaction with HBr presents the lowest reaction barrier for an O–H–Br collinear arrangement, there is a barrier height increase of only 2.23 kcal mol^{-1} when the system evolves from collinearity (180°) to 140°. This favors the existence of a substantial amount of rotational energy in products, as bent

geometries of the system are also energetically open for reaction. The corresponding barrier increase for $O(^3P)+H-(R)$ (modeling a tertiary C–H bond) is notably higher (9.95 kcal mol^{-1}), while the barrier height for the $O(^3P)+H-(CH_3)$ PES of the present work shows a dependence similar to that for the reaction with HBr, with a barrier increase of 3.48 kcal mol^{-1} when the $O-H-(CH_3)$ angle evolves from 180 to 140°. Hence, a higher rotational excitation can be expected for the OH arising from $H-(CH_3)$ than in the $H-(R)$ case. In fact, for $H-(CH_3)$ $\langle f'_R\rangle = 0.078$ (QCT, this work) and 0.118 (experimental[4]), while for $H-(R)$ $\langle f'_R\rangle$ is 0.02 (experimental,[16] see also Ref. 25 (QCT study)). The higher OH rotational excitation obtained for $O(^3P)+HBr$ when compared to that for the $O(^3P)+H-(CH_3)$ is probably due to the earlier saddle point that presents the former system (Fig. 2). If similar forces were acting on both systems, the longer OH arm of the O–H–Br case should produce a higher OH rotational excitation than in the $O-H-(CH_3)$ reaction.

IV. CONCLUDING REMARKS

An *ab initio* study of the ground potential energy surface (PES) of the $O(^3P)+CH_4 \rightarrow OH+CH_3$ reaction has been performed using the second- and fourth-order Møller–Plesset methods with large basis sets. Two saddle points ($^3A''$ and $^3A'$) and a products valley minimum ($^3A''$) have been characterized, and a set of points has been calculated to model the reaction as a triatomic system with the methyl group treated as an atom of 15.0 a.m.u. The triatomic analytical ground PES model based on a many-body expansion derived from the *ab initio* points has been employed to study the kinetics [variational transition state theory (VTST) and quasiclassical trajectory (QCT) rate constants] and dynamics (QCT method) of the reaction. The *ab initio* points have also been used directly to calculate the VTST rate constant considering all atoms of the system. When the best VTST methods are used, a good agreement is obtained with the experimental rate constant over a wide temperature range (1000–2500 K). The QCT method provides rate constant values about one-third the experimental ones within the 1500–2500 K range. The QCT OH($v'=0$) rotational distribution arising from the simulation of the reaction with $O(^3P)$ atoms produced in the photodissociation of NO_2 at 248 nm is in good agreement with experiment. The very small population of OH($v'=1$) obtained by QCT is consistent with experimental data. The results, and in particular the low OH rotational energy content, have been analyzed in terms of the microscopic reaction mechanism and also by taking into account the influence of the PES properties on the dynamics. The triatomic PES model derived in this work may be used for the study of the kinetics and dynamics of the title reaction in conditions where the motions of the methyl group are not strongly coupled to the main motions leading to reaction.

ACKNOWLEDGMENTS

This work has been supported by the ''Dirección General de Enseñanza Superior'' of the Spanish Ministry of Education and Culture through the DGES projects PB95-0598-C02-01 and PB95-0598-C02-02. J.H. thanks the CIRIT from the ''Generalitat de Catalunya'' (Autonomous Government), for a predoctoral research grant. The authors are also grateful to the ''Generalitat de Catalunya'' (Ref. DGR GRQ95-0516) and the University of La Rioja for partial support, and to the ''Centre de Supercomputació i Communicacions de Catalunya (C^4-CESCA)'' for computer time made available. Thanks are also given to Professor Donald G. Truhlar (University of Minnesota) and to a referee for helpful comments on the manuscript. Dedicated to the memory of our dear friend and colleague Dr. Francesc R. Trull.

[1] J. Warnatz, in *Combustion Chemistry*, edited by W. C. Gardiner, Jr. (Springer-Verlag, Berlin, 1984), p. 197.
[2] M. W. Chase, Jr., C. A. Davies, J. R. Downey, Jr., D. J. Frurip, R. A. McDonald, and A. N. Syverud, J. Phys. Chem. Ref. Data Suppl. 1 **14** (1985). $\Delta H^\circ_{p,298\ K}$ of O, CH_4, OH, and CH_3 are given, respectively, on pages 1639, 600, 1248, and 595.
[3] T. Suzuki and E. Hirota, J. Chem. Phys. **98**, 2387 (1993).
[4] G. M. Sweeney, A. Watson, and K. G. McKendrick, J. Chem. Phys. **106**, 9172 (1997).
[5] J. W. Sutherland, J. V. Michael, and R. B. Klemm, J. Phys. Chem. **90**, 5941 (1986).
[6] N. Cohen and K. R. Westberg, J. Phys. Chem. Ref. Data **20**, 1211 (1991).
[7] D. L. Baulch, C. J. Cobos, R. A. Cox, C. Esser, P. Frank, Th. Just, J. A. Kerr, M. J. Pilling, J. Troe, R. W. Walker, and J. Warnatz, J. Phys. Chem. Ref. Data **21**, 445 (1992), and references therein.
[8] K. Ohmori, M. Yoshimura, M. Koshi, and H. Matsui, Bull. Chem. Soc. Jpn. **65**, 1317 (1992).
[9] A. Miyoshi, K. Ohmori, K. Tsuchiya, and H. Matsui, Chem. Phys. Lett. **204**, 241 (1993).
[10] A. Miyoshi, K. Tsuchiya, N. Yamauchi, and H. Matsui, J. Phys. Chem. **98**, 11452 (1994).
[11] G. M. Sweeney and K. G. McKendrick, J. Chem. Phys. **106**, 9182 (1997).
[12] S. P. Walch and T. H. Dunning, Jr., J. Chem. Phys. **72**, 3221 (1980).
[13] C. González, J. J. W. McDouall, and H. B. Schlegel, J. Phys. Chem. **94**, 7467 (1990).
[14] B. S. Jursic, Int. J. Quantum Chem. **65**, 75 (1997).
[15] J. C. Corchado, J. Espinosa-García, O. Roberto-Neto, Y.-Y. Chuang, and D. G. Truhlar, J. Phys. Chem. A **102**, 4899 (1998).
[16] P. Andresen and A. C. Luntz, J. Chem. Phys. **72**, 5842 (1980).
[17] K. Kleinermanns and A. C. Luntz, J. Phys. Chem. **85**, 1966 (1981).
[18] K. Kleinermanns and A. C. Luntz, J. Chem. Phys. **77**, 3533 (1982).
[19] N. J. Dutton, I. W. Fletcher, and J. C. Whitehead, Mol. Phys. **52**, 475 (1984).
[20] N. J. Barry, I. W. Fletcher, and J. C. Whitehead, J. Phys. Chem. **90**, 4911 (1986).
[21] N. J. Dutton, I. W. Fletcher, and J. C. Whitehead, J. Phys. Chem. **89**, 569 (1985).
[22] K. Kleinermanns and A. C. Luntz, J. Chem. Phys. **77**, 3774 (1982).
[23] K. Kleinermanns and A. C. Luntz, J. Chem. Phys. **77**, 3537 (1982).
[24] Y. Rudich, Y. Hurwitz, S. Lifson, and R. Naaman, J. Chem. Phys. **98**, 2936 (1993).
[25] A. C. Luntz and P. Andresen, J. Chem. Phys. **72**, 5851 (1980).
[26] D. C. Clary, J. N. L. Connor, and W. J. E. Southhall, J. Chem. Phys. **84**, 2620 (1986).
[27] Y. Hurwitz, Y. Rudich, R. Naaman, and R. B. Gerber, J. Chem. Phys. **98**, 2941 (1993).
[28] R. Sayós, M. González, and A. Aguilar, Chem. Phys. **98**, 409 (1985).
[29] X. Wang, M. Ben-Nun, and R. D. Levine, Chem. Phys. **197**, 1 (1995).
[30] G. Herzberg, *Molecular Spectra and Molecular Structure* (Van Nostrand Reinhold, New York, 1966), Vol. 3.
[31] GAUSSIAN 94, Revision E.1, M. J. Frisch, G. W. Trucks, H. B. Schlegel, P. M. W. Gill, B. G. Johnson, M. A. Robb, J. R. Cheeseman, T. Keith, G. A. Petersson, J. A. Montgomery, K. Raghavachari, M. A. Al-Laham, V. G. Zakrzewski, J. V. Ortiz, J. B. Foresman, J. Cioslowski, B. B. Stefanov, A. Nanayakkara, M. Challacombe, C. Y. Peng, P. Y. Ayala, W. Chen, M. W. Wong, J. L. Andres, E. S. Replogle, R. Gomperts, R. L. Martin, D. J. Fox, J. S. Binkley, D. J. Defrees, J. Baker, J. P. Stewart, M. Head-Gordon, C. Gonzalez, and J. A. Pople, Gaussian, Inc., Pittsburgh PA, 1995.
[32] H. Arai, S. Kato, and S. Koda, J. Phys. Chem. **98**, 12 (1994).

[33] *Structure Data of Free Polyatomic Molecules*, edited by K.-H. Hellwege and A. M. Hellwege (Springer-Verlag, Berlin, 1987), Landolt-Börnstein, Vol. II/7, Suppl. Vol. 15, p. 198.
[34] M. W. Chase, Jr., C. A. Davies, J. R. Downey, Jr., D. J. Frurip, R. A. McDonald, and A. N. Syverud, J. Phys. Chem. Ref. Data Suppl. 1 **14** (1985). Experimental frequencies used for CH_4 (p. 600) and CH_3 (p. 595) to determine the heat capacity and entropy.
[35] K. P. Huber and G. Herzberg, *Molecular Spectra and Molecular Structure*, Vol. 4 (Van Nostrand Reinhold, New York, 1979), Vol. 4.
[36] *Structure Data of Free Polyatomic Molecules*, edited by K. Kuchitsu (Springer-Verlag, Berlin, 1992), Landolt-Börnstein, Vols. II/7 and II/15, Suppl. Vol. 21, p. 139.
[37] L. A. Curtiss, L. D. Kock, and J. A. Pople, J. Chem. Phys. **95**, 4040 (1991).
[38] S. F. Boys and F. Bernardi, Mol. Phys. **19**, 553 (1970).
[39] J. N. Murrell, S. Carter, S. C. Farantos, P. Huxley, and A. J. C. Varandas, *Molecular Potential Energy Surfaces* (Wiley, New York, 1984).
[40] M. González and R. Sayós, DIATOMFIT (unpublished program).
[41] R. Sayós and M. González, SM3FIT (unpublished program).
[42] M. Gilibert, A. Aguilar, M. González, F. Mota, and R. Sayós, J. Chem. Phys. **97**, 5542 (1992).
[43] M. González, J. Hijazo, J. J. Novoa, and R. Sayós, J. Chem. Phys. **105**, 10999 (1996).
[44] M. González, J. Hijazo, J. J. Novoa, and R. Sayós, J. Chem. Phys. **108**, 3168 (1998).
[45] R. Sayós, J. Hijazo, M. Gilibert, and M. González, Chem. Phys. Lett. **284**, 101 (1998).
[46] M. Broida, M. Tamir, and A. Persky, Chem. Phys. **110**, 83 (1986).
[47] D. G. Truhlar, A. D. Isaacson, and B. C. Garret, in *Theory of Chemical Reaction Dynamics*, edited by M. Baer (CRC, Boca Raton, FL, 1985), Vol. 4, p. 65.
[48] R. Steckler, Y.-Y. Chuang, E. L. Coitiño, W.-P. Hu, Y.-P. Liu, G. C. Lynch, K. A. Nguyen, C. F. Jackels, M. Z. Gu, I. Rossi, P. Fast, S. Clayton, V. S. Melissas, B. C. Garrett, A. D. Isaacson, and D. G. Truhlar, POLYRATE-version 7.0, University of Minnesota, Minneapolis, 1996.
[49] R. N. Porter and L. M. Raff, in *Dynamics of Molecular Collisions, Part B*, edited by W. H. Miller (Plenum, New York, 1976), p. 1.
[50] D. G. Truhlar and J. T. Muckerman, in *Atom-Molecule Collision Theory: A Guide for the Experimentalist*, edited by R. B. Bernstein (Plenum, New York, 1979), p. 505.
[51] H. R. Mayne, Int. Rev. Phys. Chem. **10**, 107 (1991).
[52] R. Sayós and M. González, TRIQCT (unpublished program).
[53] S. Bashkin and J. O. Stoner, *Atomic Energy Levels and Grotrian Diagrams* (Elsevier, New York, 1975), p. 165.
[54] J. McFarlane, J. C. Polanyi, and J. G. Shapter, J. Photochem. Photobiol., A **58**, 139 (1991).
[55] R. W. Quandt, X. Wang, K. Tsukiyama, and R. Bersohn, Chem. Phys. Lett. **276**, 122 (1997).
[56] K. G. McKendrick, D. J. Rakestraw, R. Zhang, and R. N. Zare, J. Phys. Chem. **92**, 5530 (1988).